# Heat Capacities and Nonisothermal Thermal Decomposition Reaction Kinetics of D-Mannitol

**Bo Tong,[†] Rui-Bin Liu,[†] Chang-Gong Meng,[†] Feng-Yun Yu,[‡] Shou-Hua Ji,[‡] and Zhi-Cheng Tan*[,§]**

Department of Chemistry, School of Chemical Engineering, Dalian University of Technology, Dalian 116023, China, Material Testing Center, Dalian University of Technology, Dalian 116023, China, and Thermochemistry Laboratory, Dalian Institute of Chemical Physics, Chinese Academy of Sciences, Dalian 116023, China

The low-temperature heat capacity $C_{p,m}$ of D-mannitol was measured in the temperature range from (80 to 390) K by means of a fully automated adiabatic calorimeter. The dependence of heat capacity on the temperature was fitted to a polynomial equation with the least-squares method. The thermodynamic functions ($H_T - H_{298.15\ K}$) and ($S_T - S_{298.15\ K}$) were derived from the heat capacity data in the temperature range of (80 to 390) K with an interval of 5 K. The melting temperature, molar enthalpy, and entropy of fusion were determined to be (437.25 ± 0.12) K, (54.69 ± 1.64) kJ·mol$^{-1}$, and (125.08 ± 3.75) J·K$^{-1}$·mol$^{-1}$ by DSC measurements. The thermal stability and nonisothermal thermal decomposition kinetics of the compound were studied by the TG-DTG technique under atmospheric pressure and flowing nitrogen gas conditions. The thermal decomposition process had one mass loss stage, and the apparent activation energy $E_a$ was obtained to be (120.61 ± 1.85) kJ·mol$^{-1}$ by the Kissinger, Friedman, and Flynn−Wall−Ozawa methods. The Malek method was used to identify the most probable kinetic model SB($m$, $n$). The kinetics model function and the pre-exponential factor $A$ were expressed to be: $f(\alpha) = \alpha^{0.306}(1 - \alpha)^{0.381}$; ln $A = 17.88$, respectively.

## Introduction

Natural polyols such as xylitol, sorbitol, erythritol, and adonitol are low molecular weight carbohydrates that are significant to food and pharmaceutical industries. Due to the characteristic sweet taste and low energy (Joule) content compared with sucrose, they are increasingly used to provide sweetness for various drugs or replace sugars in confectionery.[1−3] Moreover, they reduce the development of dental caries and do not require insulin in their metabolism, so they are suitable for diabetics. Furthermore, they are natural extracts that have more advantages, such as nontoxic, no erosion, and no environmental pollution, than other polyols.[4−6]

For industrial and pharmaceutical applications, the state and phase transitions of drugs are very important because they reflect molecular mobility and physicochemical properties that have a direct effect on the formation and changes of structure, time-dependent crystallization, and product shelf life.[7,8] It is now recognized that the amorphous solid state offers very interesting possibilities in the control of bioavailability.[9,10] Therefore, knowledge of the thermodynamic properties such as heat capacities, phase transition, and thermal decomposing process is an important requirement for safe storage and use of these natural polyols.

As a continuation of our series research work on thermodynamic properties of natural polyols,[11,12] in the present study, the thermodynamic properties of D-mannitol including the heat capacity, melting temperature, entropy, and enthalpy of fusion were investigated by adiabatic calorimetry (AC) and differential scanning calorimetry (DSC). The thermostability and nonisothermal thermal decomposition reaction kinetics were studied by TG-DTG, and the kinetic model was established by the Malek method.

* Corresponding author. E-mail: tzc@dicp.ac.cn. Fax: +86-411-84691570. Tel.: +86-411-84379199.
[†] School of Chemical Engineering, Dalian University of Technology.
[‡] Material Testing Center, Dalian University of Technology.
[§] Dalian Institute of Chemical Physics, Chinese Academy of Sciences.

## Experimental Section

The D-Mannitol [CAS No. 69-65-8] was purchased from Tianjin Chemical Engineering Institute, in PR China, with labeled purity of 99.0 % mass fraction. The sample was purified by recrystallization and sublimation, and the final purity was 99.9 % mass fraction. It was handled in a dry $N_2$ atmosphere to avoid possible contamination by moisture.

Heat capacity measurements were carried out in a high-precision automated adiabatic calorimeter described in detail in the literature.[13−15] The calorimeter was established by the Thermochemistry Laboratory of Dalian Institute of Chemical Physics, Chinese Academy of Sciences, in PR China. To verify the reliability of the adiabatic calorimeter, the molar heat capacities for the reference standard material α-$Al_2O_3$ were measured. The relative deviations of our experimental results from the recommended values by NIST[16] were within ± 0.2 % in the entire temperature range of (80 to 390) K. The sample mass used for the heat capacity measurement is 3.54128 g, which is equivalent to 19.439 mmol based on its molar mass of 182.17 g·mol$^{-1}$.

A differential scanning calorimeter (model: DSC141, SETARAM, France) was used to perform the thermal analysis of D-mannitol under high purity nitrogen (99.999 %) with a flow rate of 40 mL·min$^{-1}$. The sample mass of (3 to 5) mg was filled and pressed into an alumina crucible. Three experimental tests were performed at heating rate of 10 K·min$^{-1}$ with α-$Al_2O_3$ as the reference material.

The TG measurements of the sample were carried out by a thermogravimetric analyzer (model: TGA/ SDTA 851$^e$, Mettler Toledo, Switzerland) under $N_2$ with a flow rate of 40 mL·min$^{-1}$ at the heating rate of (5, 10, 15, 20, and 25) K·min$^{-1}$ from (300

10.1021/je900285w CCC: $40.75 
Published on Web 07/16/2009

**Table 1. Experimental Molar Heat Capacities of D-Mannitol ($M$ = 182.17 g·mol$^{-1}$)**

| $T$ | $C_{p,m}$ | $T$ | $C_{p,m}$ | $T$ | $C_{p,m}$ |
|---|---|---|---|---|---|
| K | J·K$^{-1}$·mol$^{-1}$ | K | J·K$^{-1}$·mol$^{-1}$ | K | J·K$^{-1}$·mol$^{-1}$ |
| 80.423 | 71.86 | 183.607 | 159.2 | 288.450 | 253.1 |
| 84.120 | 75.82 | 186.661 | 162.1 | 291.426 | 256.0 |
| 87.056 | 79.00 | 189.701 | 165.0 | 294.392 | 259.0 |
| 90.044 | 82.17 | 192.754 | 168.2 | 297.492 | 260.6 |
| 93.087 | 85.24 | 195.811 | 170.5 | 300.607 | 262.6 |
| 96.038 | 88.00 | 198.931 | 173.9 | 303.635 | 264.9 |
| 99.046 | 90.89 | 202.132 | 176.6 | 306.662 | 266.7 |
| 102.114 | 93.72 | 205.296 | 180.9 | 309.687 | 268.4 |
| 105.110 | 96.44 | 208.404 | 184.3 | 312.777 | 270.6 |
| 108.048 | 98.92 | 211.462 | 187.3 | 315.921 | 272.9 |
| 111.055 | 101.4 | 214.486 | 189.7 | 319.056 | 275.3 |
| 114.135 | 104.0 | 217.577 | 192.1 | 322.187 | 277.9 |
| 117.157 | 106.5 | 220.743 | 195.4 | 325.301 | 280.3 |
| 120.114 | 109.0 | 223.878 | 198.8 | 328.401 | 282.6 |
| 123.128 | 111.5 | 226.994 | 202.7 | 331.486 | 284.8 |
| 126.215 | 113.8 | 230.035 | 204.2 | 334.561 | 286.1 |
| 129.264 | 116.1 | 233.085 | 207.6 | 337.627 | 289.0 |
| 132.272 | 118.9 | 236.153 | 210.5 | 340.677 | 291.4 |
| 135.239 | 120.9 | 239.218 | 213.4 | 343.777 | 293.3 |
| 138.177 | 123.0 | 242.239 | 215.7 | 346.921 | 295.5 |
| 141.200 | 125.4 | 245.326 | 217.7 | 350.053 | 297.6 |
| 144.278 | 127.8 | 248.419 | 220.0 | 353.164 | 299.6 |
| 147.310 | 129.9 | 251.418 | 221.4 | 356.265 | 301.3 |
| 150.305 | 132.2 | 254.484 | 223.2 | 359.310 | 303.7 |
| 153.283 | 134.4 | 257.613 | 226.2 | 362.514 | 305.8 |
| 156.234 | 136.7 | 260.729 | 228.0 | 365.683 | 308.4 |
| 159.247 | 138.8 | 263.828 | 230.7 | 368.863 | 310.2 |
| 162.366 | 141.7 | 266.983 | 233.6 | 372.042 | 311.9 |
| 165.486 | 143.2 | 270.148 | 236.1 | 375.210 | 314.0 |
| 168.579 | 146.4 | 273.218 | 239.5 | 378.348 | 316.7 |
| 171.607 | 149.2 | 276.280 | 242.1 | 381.444 | 319.0 |
| 174.593 | 150.8 | 279.347 | 245.4 | 384.520 | 320.9 |
| 177.598 | 152.9 | 282.412 | 248.6 | 387.645 | 322.7 |
| 180.587 | 156.6 | 285.438 | 251.6 | | |

to 800) K, respectively. The sample mass of (9.91, 10.30, 9.73, 12.16, and 11.83) mg corresponding to the above heating rate, respectively, was filled into an alumina crucible without pressing.

## Results and Discussion

***Low-Temperature Heat Capacity and Thermodynamic Function.*** Experimental molar heat capacities of D-mannitol measured by the adiabatic calorimeter over the temperature range from (80 to 390) K are listed in Table 1 and plotted in Figure 1. From Figure 1, a smoothed curve with no endothermic or exothermic peaks was obtained in the experimental temperature range, which indicated that the sample was thermostable from the liquid nitrogen temperature to 400 K. The values of experimental heat capacities were fitted to the following polynomial equations with the least-squares method[17,18]

$$C_{p,m}/\mathrm{J\cdot K^{-1}\cdot mol^{-1}} = 207.790 + 141.210x - 23.623x^2 - 38.543x^3 + 44.992x^4 + 23.902x^5 - 32.126x^6 \quad (1)$$

where $x$ is the reduced temperature

$$x = [T - (T_{max} + T_{min})/2]/[(T_{max} - T_{min})/2] \quad (2)$$

In the above equation, $T_{max}$ and $T_{min}$ are the upper (390 K) and lower (80 K) limit of the experimental temperature range, respectively. The correlation coefficient of the fitting $r^2$ = 0.9999.

The thermodynamic functions ($H_T - H_{298.15}$) and ($S_T - S_{298.15}$) of the D-mannitol relative to the reference temperature 298.15 K were calculated in the temperature range (80 to 390) K with an interval of 5 K, using the polynomial equation of heat capacity and thermodynamic relationships as follows

$$H_T - H_{298.15} = \int_{298.15}^{T} C_{p,m}\mathrm{d}T \quad (3)$$

$$S_T - S_{298.15} = \int_{298.15}^{T} \frac{C_{p,m}}{T}\mathrm{d}T \quad (4)$$

The calculated results are listed in Table 2.

***Temperature, Enthalpy, and Entropy of Fusion Determined by DSC.*** One of DSC curves was shown in Figure 2. From the figure, a sharply endothermic peak corresponding to the melting process was observed with an onset point of 437.25 K and a peak temperature of 442.76 K. The mean values of three measurements were determined to be: melting temperature (437.25 ± 0.12) K, molar enthalpy of fusion (54.69 ± 1.64) kJ·mol$^{-1}$, and entropy of fusion (125.08 ± 0.38) J·K$^{-1}$·mol$^{-1}$, respectively.

***Thermostability Determined by TG-DTG.*** The TG-DTG curves in nonisothermal conditions shown in Figure 3 are obtained at various heating rates. From Figure 3, it can be seen that the mass loss of the sample was completed in a single step. The sample keeps thermostable below 500 K. It begins to lose

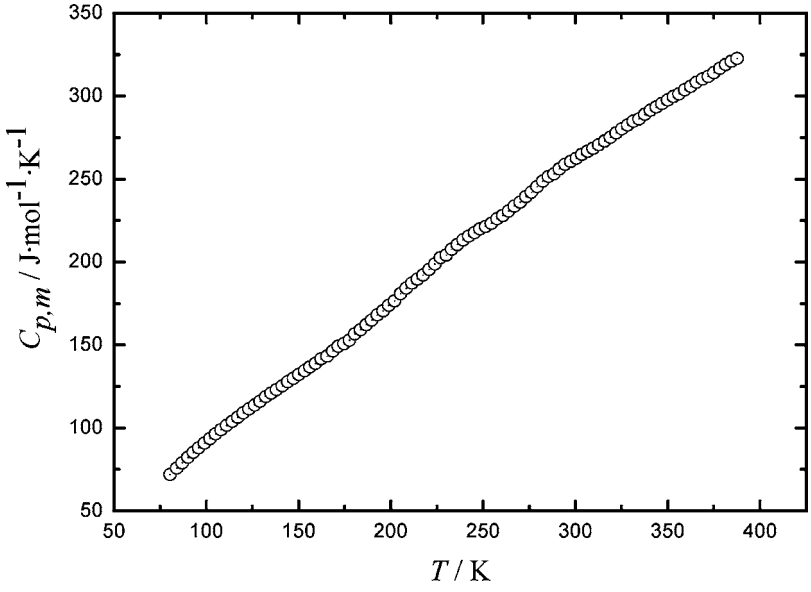


**Figure 1.** Experimental molar heat capacity $C_{p,m}$ of D-mannitol as a function of temperature.

**Table 2. Smoothed Heat Capacities and Thermodynamic Functions of D-Mannitol ($M$ = 182.17 g·mol$^{-1}$)**

| $T$/K | $C_{p,m}$/J·K$^{-1}$·mol$^{-1}$ | $H_T - H_{298.15}$/kJ·mol$^{-1}$ | $S_T - S_{298.15}$/J·K$^{-1}$mol$^{-1}$ | $T$/K | $C_{p,m}$/J·K$^{-1}$mol$^{-1}$ | $H_T - H_{298.15}$/kJ·mol$^{-1}$ | $S_T - S_{298.15}$/J·K$^{-1}$mol$^{-1}$ |
|---|---|---|---|---|---|---|---|
| 80 | 70.46 | −36.43 | −193.4 | 240 | 212.3 | −13.78 | −51.30 |
| 85 | 76.73 | −36.07 | −188.9 | 245 | 216.8 | −12.71 | −46.87 |
| 90 | 82.37 | −35.67 | −184.4 | 250 | 221.2 | −11.61 | −42.44 |
| 95 | 87.51 | −35.24 | −179.8 | 255 | 225.5 | −10.50 | −38.01 |
| 100 | 92.23 | −34.79 | −175.2 | 260 | 229.8 | −9.358 | −33.58 |
| 105 | 96.64 | −34.32 | −170.6 | 265 | 234.0 | −8.199 | −29.15 |
| 110 | 100.8 | −33.83 | −166.0 | 270 | 238.2 | −7.018 | −24.73 |
| 115 | 104.8 | −33.31 | −161.5 | 275 | 242.2 | −5.817 | −20.31 |
| 120 | 108.7 | −32.78 | −156.9 | 280 | 246.2 | −4.596 | −15.91 |
| 125 | 112.5 | −32.23 | −152.4 | 285 | 250.1 | −3.356 | −11.51 |
| 130 | 116.2 | −31.66 | −147.9 | 290 | 254.0 | −2.095 | −7.124 |
| 135 | 120.0 | −31.07 | −143.4 | 295 | 257.8 | −0.816 | −2.749 |
| 140 | 123.8 | −30.46 | −139.0 | 298.15 | 260.2 | 0.000 | 0.000 |
| 145 | 127.7 | −29.83 | −134.6 | 300 | 261.5 | 0.483 | 1.612 |
| 150 | 131.6 | −29.18 | −130.2 | 305 | 265.2 | 1.800 | 5.962 |
| 155 | 135.6 | −28.51 | −125.8 | 310 | 268.9 | 3.135 | 10.30 |
| 160 | 139.7 | −27.82 | −121.4 | 315 | 272.5 | 4.489 | 14.62 |
| 165 | 143.9 | −27.11 | −117.0 | 320 | 276.1 | 5.860 | 18.93 |
| 170 | 148.2 | −26.38 | −112.7 | 325 | 279.7 | 7.250 | 23.23 |
| 175 | 152.5 | −25.63 | −108.3 | 330 | 283.3 | 8.658 | 27.52 |
| 180 | 156.9 | −24.86 | −104.0 | 335 | 286.9 | 10.08 | 31.80 |
| 185 | 161.4 | −24.06 | −99.61 | 340 | 290.4 | 11.53 | 36.08 |
| 190 | 166.0 | −23.24 | −95.25 | 345 | 293.9 | 12.99 | 40.34 |
| 195 | 170.6 | −22.40 | −90.89 | 350 | 297.5 | 14.47 | 44.59 |
| 200 | 175.2 | −21.54 | −86.52 | 355 | 301.0 | 15.96 | 48.84 |
| 205 | 179.9 | −20.65 | −82.15 | 360 | 304.4 | 17.48 | 53.08 |
| 210 | 184.6 | −19.74 | −77.76 | 365 | 307.9 | 19.01 | 57.32 |
| 215 | 189.3 | −18.80 | −73.37 | 370 | 311.2 | 20.55 | 61.54 |
| 220 | 193.9 | −17.85 | −68.97 | 375 | 314.5 | 22.12 | 65.75 |
| 225 | 198.6 | −16.86 | −64.57 | 380 | 317.7 | 23.70 | 69.94 |
| 230 | 203.2 | −15.86 | −60.15 | 385 | 320.7 | 25.30 | 74.11 |
| 235 | 207.8 | −14.83 | −55.73 | 390 | 323.6 | 26.91 | 78.25 |

**Table 3. Peak Temperature of Decomposition for D-Mannitol Obtained by TG-DTG Curves Corresponding to Various Heating Rates and the Calculated Result by the Kissinger Method**

| $\beta$/K·min$^{-1}$ | 5 | 10 | 15 | 20 | 25 |
|---|---|---|---|---|---|
| $T_p$/K | 622.848 | 642.093 | 650.547 | 657.801 | 667.355 |

$E_a$ = 118.42; $r^2$ = 0.9960

mass at about 540 K, reaches the maximum rate of mass loss at about 650 K, and completely loses its mass when the temperature reaches 700 K. The values of the temperatures are slightly different depending on the various heating rates from (5 to 25) K·min$^{-1}$.

***Apparent Activation Energy.*** Kissinger, Flynn−Wall−Ozawa, and Friedman methods[19−21] were used to calculate apparent activation energy ($E_a$) of the thermal decomposition reaction for D-mannitol.

Kissinger equation

$$\ln \frac{\beta}{T^2} = \ln \frac{AR}{E_a} - \frac{E_a}{R}\frac{1}{T} \tag{5}$$

Flynn−Wall−Ozawa equation

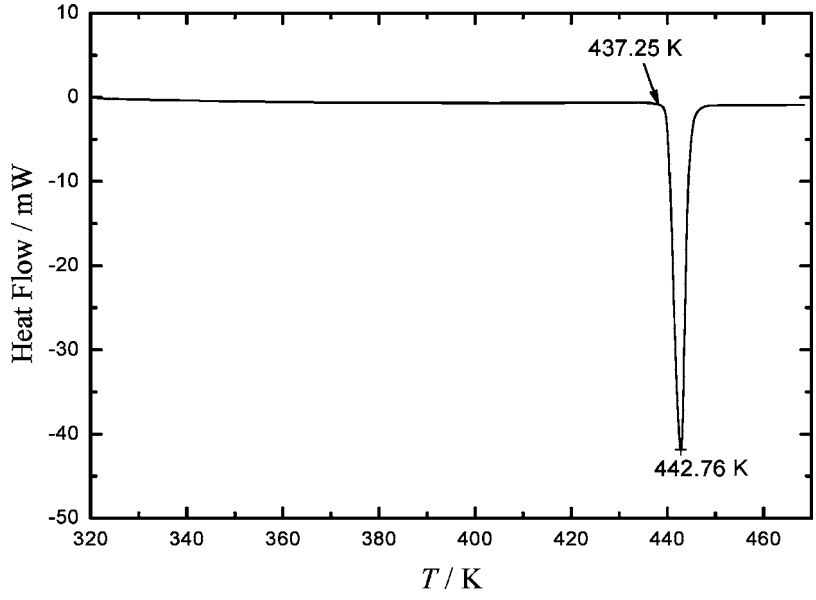


**Figure 2.** DSC curve of D-manitol under high purity nitrogen.

$$\ln \beta = \ln\left(\frac{AE_a}{RG(\alpha)}\right) - 5.3305 - 1.0516\frac{E_a}{R}\frac{1}{T} \qquad (6)$$

Friedman equation

$$\ln\left(\frac{\beta d\alpha}{dT}\right) = \ln[Af(\alpha)] - \frac{E_a}{R}\frac{1}{T} \qquad (7)$$

where $\beta$ is the heating rate; $A$ is the pre-exponential factor; $R$ is the gas constant; $T$ is the absolute temperature; $G(\alpha)$ is the integral mechanism function; and $\alpha$ is the conversion degree, respectively.

$$\alpha = \frac{m_0 - m_T}{m_0 - m_\infty} \qquad (8)$$

where $m_T$ is the mass at temperature $T$; $m_0$ is the initial sample mass; and $m_\infty$ is the mass at the end of experiments, respectively.

The peak temperature $T_p$ of the exothermic decomposition reaction for D-mannitol determined by the TG-DTG curve was listed in Table 3. According to the Kissinger method (eq 5), the curve of $\ln(\beta/T_p^2)$ versus $10^3/T$ was plotted in Figure 4, and $E_a$ was calculated to be 118.42 kJ·mol$^{-1}$ by the slope of the curve with correlation coefficient $r^2 = 0.9919$.[19,22]

By substituting the original data, $\beta_i$, $T_i$, and $\alpha_i$ ($i = 1,2, ...,n$), tabulated in Table 4 from TG-DTG curves into eq 6, the values of $E_a$ for any given value of $\alpha$ in Table 4 were obtained. The curve of $\ln \beta$ to $10^3/T$ was plotted in Figure 5, and the average value of $E_a$ in the range of 0.10 to 0.80 was 124.28 kJ·mol$^{-1}$ according to the Flynn−Wall−Ozawa method[20,23] with the correlation coefficient $r^2 = 0.9821$, 0.9870, 0.9885, 0.9892, 0.9894, 0.9894, 0.9889, and 0.9883, respectively.

By substituting the original data into eq 7 ($0.3 \le \alpha \le 0.7$), the values of $E_a$ for different heating rates $\beta$ in Table 5 were obtained. The average value of $E_a$ was 119.14 kJ·mol$^{-1}$ according to the Friedman method.

Then, $E_a$ was determined to be (120.61 ± 1.85) kJ·mol$^{-1}$ which was the mean value obtained by the three methods.[21,24]

***Most Probable Kinetic Model and Pre-Exponential Fator.*** The following eq 9 was used for kinetic analysis of solid-state decompositions.[25]

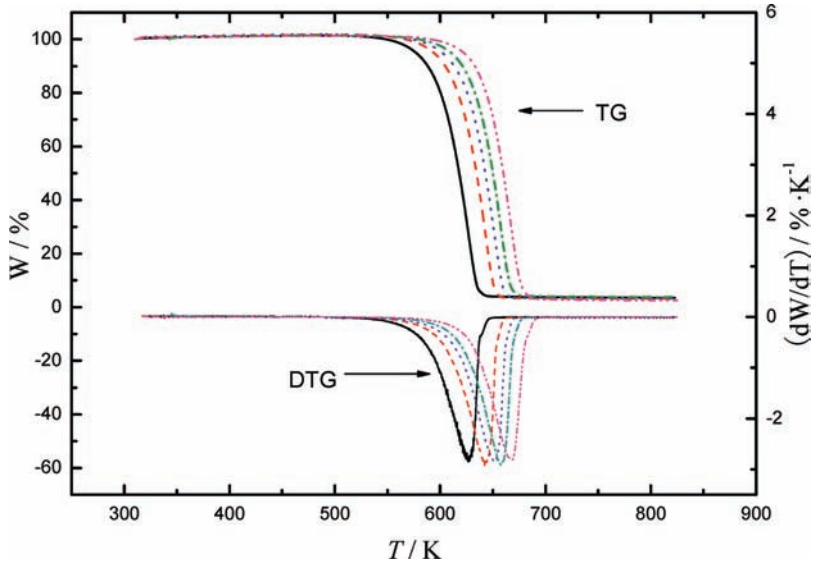


**Figure 3.** TG-DTG curve of D-manitol under high purity nitrogen at different heating rates. *W* is mass loss of the sample in percent.

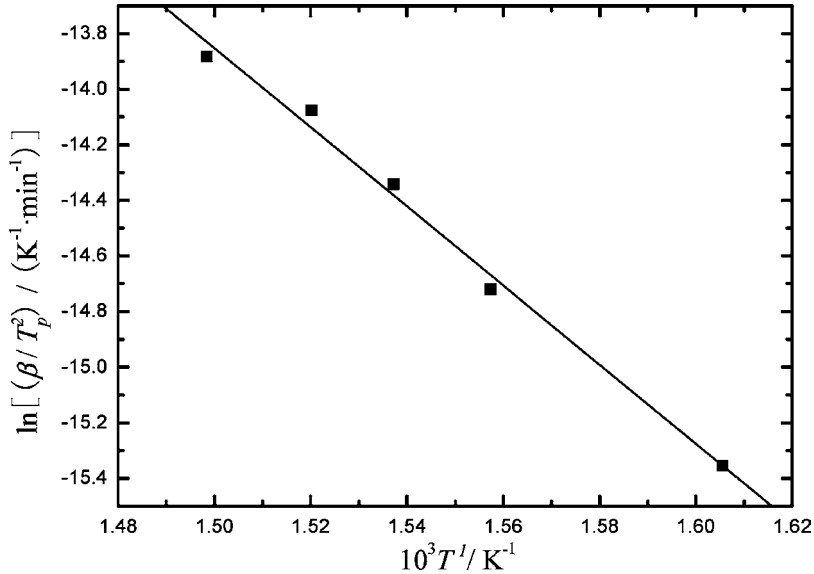


**Figure 4.** Curve of $\ln(\beta T_p^{-2})$ versus $10^3/T$. $y = 7.51329 - 14.24341x$; $r^2 = 0.9919$.

$$\frac{d\alpha}{dt} = A\exp\left(-\frac{E_a}{RT}\right)f(\alpha) \quad (9)$$

where $t$ is the time. Under nonisothermal conditions in which samples are heated at a constant rate, the following was obtained

$$\frac{d\alpha}{dT} = \frac{A}{\beta}\exp\left(-\frac{E_a}{RT}\right)f(\alpha) \quad (10)$$

Once the activation energy has been determined, the Malek method[25−28] was used to find the most probable kinetic model which best described the measure set of TG data. Two special functions $y(\alpha)$ and $z(\alpha)$ were defined and expressed as follows

$$y(\alpha) = \left(\frac{d\alpha}{dt}\right)e^x = Af(\alpha) \quad (11)$$

$$z(\alpha) = \pi(x)\left(\frac{d\alpha}{dt}\right)\frac{T}{\beta} \quad (12)$$

where $x = E_a/RT$ and $\pi(x)$[28] is an approximation of the temperature integral.

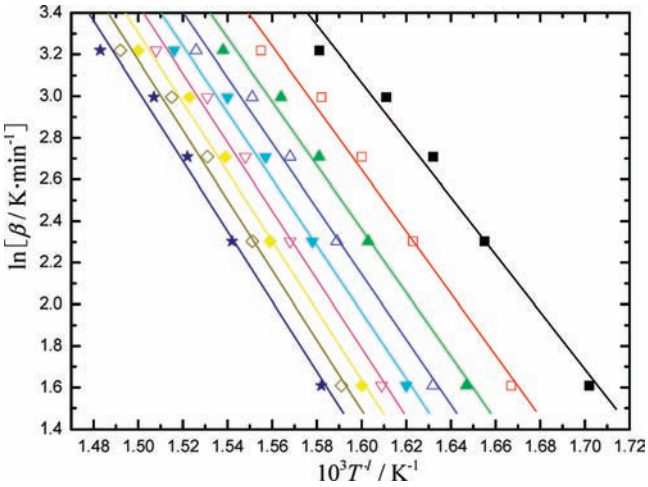


**Figure 5.** Curve of ln($\beta$) versus $10^3/T$ at various conversion degree. ■, 0.1; □, 0.2; ▲, 0.3; △, 0.4; ▼, 0.5; ▽, 0.6; ♦, 0.7; ◇, 0.8; ★, 0.9.

**Table 4. Experimental and Calculated Data by the Flynn−Wall−Ozawa Method**

| | $\beta = 5$ K·min$^{-1}$ | $\beta = 10$ K·min$^{-1}$ | $\beta = 15$ K·min$^{-1}$ | $\beta = 20$ K·min$^{-1}$ | $\beta = 25$ K·min$^{-1}$ | $E_a$ |
|---|---|---|---|---|---|---|
| α | $T_i$/K | $T_i$/K | $T_i$/K | $T_i$/K | $T_i$/K | kJ·mol$^{-1}$ |
| 0.10 | 587.621 | 604.370 | 612.776 | 620.653 | 632.538 | 109.07 |
| 0.15 | 594.641 | 611.221 | 619.951 | 627.359 | 638.713 | 113.50 |
| 0.20 | 599.770 | 616.261 | 625.107 | 632.285 | 643.288 | 116.68 |
| 0.25 | 603.835 | 620.329 | 629.124 | 636.230 | 646.995 | 119.12 |
| 0.30 | 607.217 | 623.742 | 632.460 | 639.541 | 650.119 | 121.08 |
| 0.35 | 610.152 | 626.669 | 635.340 | 642.418 | 652.850 | 122.73 |
| 0.40 | 612.790 | 629.320 | 637.879 | 644.946 | 655.261 | 124.39 |
| 0.45 | 615.174 | 631.685 | 640.183 | 647.226 | 657.465 | 125.74 |
| 0.50 | 617.392 | 633.858 | 642.307 | 649.343 | 659.511 | 127.20 |
| 0.55 | 619.440 | 635.867 | 644.300 | 651.306 | 661.429 | 128.38 |
| 0.60 | 621.399 | 637.761 | 646.180 | 653.152 | 663.273 | 129.51 |
| 0.65 | 623.252 | 639.565 | 647.989 | 654.898 | 665.050 | 130.51 |
| 0.70 | 625.031 | 641.302 | 649.722 | 656.596 | 666.804 | 131.34 |
| 0.75 | 626.771 | 642.986 | 651.430 | 658.251 | 668.539 | 132.09 |
| 0.80 | 628.519 | 644.687 | 653.147 | 659.940 | 670.282 | 132.84 |
| 0.85 | 630.306 | 646.438 | 654.916 | 661.662 | 672.174 | 133.32 |
| 0.90 | 632.230 | 648.326 | 656.834 | 663.616 | 674.423 | 133.20 |

$E_a = 124.28$ kJ·mol$^{-1}$ ($0.1 \le \alpha \le 0.8$); $\sigma = 1.85$

**Table 5. Experimental and Calculated Data by the Friedman Method**

| $\beta$/K·min$^{-1}$ | 5 | 10 | 15 | 20 | 25 |
|---|---|---|---|---|---|
| $E_a$/kJ·mol$^{-1}$ | 113.31 | 120.99 | 117.56 | 127.62 | 116.21 |

$E_a = 119.14$ kJ·mol$^{-1}$ ($0.3 \le \alpha \le 0.7$); $\sigma = 2.45$

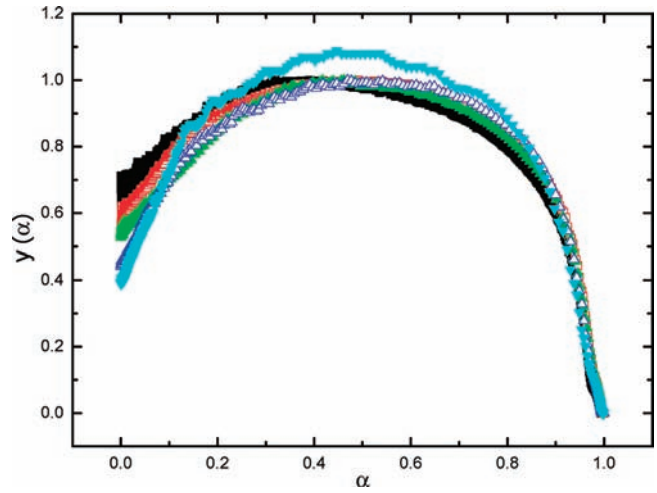


**Figure 6.** $y(\alpha)$ versus α curves at various heating rates. ■, 5 K·min$^{-1}$; □, 10 K·min$^{-1}$; ▲, 15 K·min$^{-1}$; △, 20 K·min$^{-1}$; ▼, 25 K·min$^{-1}$.

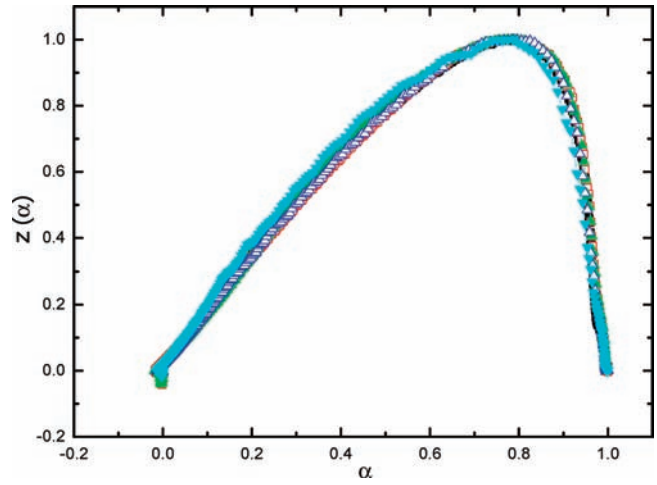


**Figure 7.** $z(\alpha)$ versus α curves at various heating rates. ■, 5 K·min$^{-1}$; □, 10 K·min$^{-1}$; ▲, 15 K·min$^{-1}$; △, 20 K·min$^{-1}$; ▼, 25 K·min$^{-1}$.

**Table 6. Values of $\alpha_m$, $\alpha_p^\infty$, and $s$ at Different Heating Rates ($\beta$)**

| $\beta$/K·min$^{-1}$ | $\alpha_m$ | $\alpha_p^\infty$ | $s$ |
|---|---|---|---|
| 5 | 0.320 | 0.783 | 0.470 |
| 10 | 0.491 | 0.757 | 0.966 |
| 15 | 0.461 | 0.775 | 0.857 |
| 20 | 0.469 | 0.786 | 0.884 |
| 25 | 0.447 | 0.752 | 0.809 |

Figures 6 and 7 were obtained by substituting the experimental data of TG-DTG to eq 11 and eq 12, respectively. The values of $\alpha_m$ and $\alpha_p^\infty$ corresponding to the maxima of both $y(\alpha)$ and $z(\alpha)$ curves were summarized in Table 6. It is evident that the values of these important parameters conform to the SB($m$, $n$) model,[25−28] which is known as

$$f(\alpha) = \alpha^m(1-\alpha)^n \quad (13)$$

The kinetic parameter ratio $s = m/n$ can be calculated using the equation. $m$ and $n$ are the first and second kinetic exponent, respectively.

Then, eq 9 may be expressed in the form

$$\ln\left[\frac{d\alpha}{dt}\exp\left(\frac{E}{RT}\right)\right] = \ln A + n\ln[\alpha^s(1-\alpha)] \quad (14)$$

The kinetic parameter $n$ and ln $A$ correspond to the slope and intercept of linear dependence of ln[(d$\alpha$/d$t$) exp($E$/$RT$)] versus ln[$\alpha^s(1-\alpha)$], respectively.

**Table 7. Kinetic Parameters Obtained Using the Malek Method at Different Heating Rates ($\beta$) ($E_a = 120.61 \pm 1.85$ kJ·mol$^{-1}$)**

| $\beta$/K·min$^{-1}$ | $m$ | $n$ | ln($A$/min$^{-1}$) |
|---|---|---|---|
| 5 | 0.163 | 0.346 | 17.63 |
| 10 | 0.377 | 0.390 | 17.89 |
| 15 | 0.316 | 0.369 | 17.95 |
| 20 | 0.314 | 0.355 | 17.99 |
| 25 | 0.362 | 0.448 | 17.97 |
| mean | 0.306 | 0.381 | 17.88 |

Then the second kinetic exponent is $m = s{\cdot}n$. The results calculated are shown in Table 7. Taking these values we can calculate average kinetic parameters for the decomposition of D-mannitol as $E_a = (120.61 \pm 1.85)$ kJ·mol$^{-1}$, ln $A = 17.88$, $m = 0.306$, and $n = 0.381$, and the kinetic model function can be expressed as

$$f(\alpha) = \alpha^{0.306}(1 - \alpha)^{0.381}$$

## Conclusions

The heat capacities and the thermodynamic functions of D-mannitol are measured in the temperature range from (80 to 390) K by a high-precision automated adiabatic calorimeter. The melting temperature, standard molar enthalpy, and entropy of fusion are determined to be (437.25 ± 0.12) K, (54.69 ± 1.64) kJ·mol$^{-1}$, and (125.08 ± 0.38) J·K$^{-1}$·mol$^{-1}$, respectively, by DSC analysis. The thermal stability and nonisothermal thermal decomposition kinetics of the compound are studied by TG-DTG measurements under atmospheric pressure and flowing nitrogen gas conditions. The thermal decomposition process has one mass loss stage, and the apparent activation energy $E_a$ is obtained to be (120.61 ± 1.85) kJ·mol$^{-1}$ by Kissinger, Friedman, and Flynn−Wall−Ozawa methods. The Malek method is used to identify the most probable kinetic model SB($m$, $n$). The kinetics model function and the pre-exponential factor $A$ are expressed to be $f(\alpha) = \alpha^{0.306}(1 - \alpha)^{0.381}$ and ln $A = 17.88$ min$^{-1}$, respectively.

## Literature Cited


(1) Voragen, A. G. J. Technological aspects of functional food-related carbohydrates. *Trends Food. Sci. Technol.* **1998**, *9*, 328–335.

(2) Talja, R. A.; Roos, Y. H. Phase and state transition effects on dielectric, mechanical, and thermal properties of polyols. *Thermochim. Acta* **2001**, *38*, 109–121.

(3) Marti, N.; Funes, L. L.; Saura, D.; Micol, V. An update on alternative sweetness. *Int. Sugar J.* **2008**, *110*, 425–429.

(4) Kroger, M.; Meister, K.; Kava, R. Low-calorie sweeteners and other sugar substitutes: A review of the safety issues. *Compr. Rev. Food. Sci. F* **2006**, *5*, 35–47.

(5) Bellisle, F.; Drewnowski, A. Intense sweeteners, energy intake and the control of body weight. *Eur. J. Clin. Nutr.* **2007**, *61*, 691–700.

(6) Duffy, V. B.; Sigman-Grant, M. Position of the American Dietetic Association: Use of nutritive and nonnutritive sweeteners. *J. Am. Diet. Assoc.* **2004**, *104*, 255–275.

(7) Steenwijk, J.; Langerock, R.; van Es, D. S.; van Haveren, J.; Geus, J. W.; Jenneskens, L. W. Long-term heat stabilisation by (natural) polyols in heavy metal- and zinc-free poly(vinyl chloride). *Polym. Degrad. Stab.* **2006**, *91*, 52–59.

(8) Diogo, H. P.; Pintoa, S. S.; Moura Ramosb, J. J. Slow molecular mobility in the crystalline and amorphous solid states of pentitols: a study by thermally stimulated depolarisation currents and by differential scanning calorimetry. *Carbohydr. Res.* **2007**, *342*, 961–969.

(9) Hancock, B. C.; York, P.; Rove, R. C. The use of solubility parameters in pharmaceutical dosage form design. *J. Pharm. Sci.* **1997**, *148*, 1–21.

(10) Craig, D. Q. M.; Royal, P. G.; Kett, V. L.; Hopton, M. L. The relevance of the amorphous state to pharmaceutical dosage forms: glassy drugs and freeze dried systems. *Int. J. Pharm.* **1999**, *179*, 179–207.

(11) Tong, B.; Tan, Z. C.; Shi, Q.; Li, Y. S.; Yue, D. T.; Wang, S. X. Thermodynamic investigation of several natural polyols (I): Heat capacities and thermodynamic properties of xylitol. *Thermochim. Acta* **2007**, *457*, 20–26.

(12) Tong, B.; Tan, Z. C.; Shi, Q.; Li, Y. S.; Wang, S. X. Thermodynamic investigation of several natural polyols (II) - Heat capacities and thermodynamic properties of sorbitol. *J. Therm. Anal. Calorim.* **2008**, *91*, 463–469.

(13) Tan, Z. C.; Sun, G. Y.; Sun, Y. J. An Adiabatic Low-temperature Calorimeter Foe Heat-capacity Measurement of Small Samples. *J. Therm. Anal. Calorim.* **1995**, *45*, 59–67.

(14) Tan, Z. C.; Sun, G. Y; Song, Y. J.; Wang, L.; Han, J. R.; Liu, Y. S.; Wang, M.; Nie, D. Z. An adiabatic calorimeter for heat capacity measurements of small samples-The heat capacity of nonlinear optical materials $KTiOPO_4$ and $RbTiOAsO_4$ Crystals. *Thermochim. Acta* **2000**, *352*, 247–253.

(15) Tan, Z. C.; Sun, L. X.; Meng, S. H.; Li, L.; Xu, F.; Yu, P.; Liu, B. P.; Zhang, J. B. Heat capacities and thermodynamic functions of p-chlorobenzoic acid. *J. Chem. Thermodyn.* **2002**, *34*, 1417–1429.

(16) Archer, D. G. Thermodynamic properties of synthetic sapphire ($\alpha$-$Al_2O_3$), standard reference material 720 and the effect of temperature-scale differences on thermodynamic properties. *J. Phys. Chem. Ref. Data.* **1993**, *22*, 1411–1453.

(17) Guo, J. P.; Liu, B. P.; Lv, X. C.; Tan, Z. C; Tong, B.; Shi, Q.; Wang, D. F. Molar heat capacities, thermodynamic properties, and thermal stability of trans-4-(aminomethyl)cyclohexanecarboxylic acid. *J. Chem. Eng. Data* **2007**, *52*, 1678–1680.

(18) Wang, M. H.; Tan, Z. C.; Sun, X. H.; Zhang, H. T.; Liu, B. P.; Sun, L. X.; Zhang, T. Determination of Heat Capacities and Thermodynamic Properties of 2-(Chloromethylthio) benzothiazole by an Adiabatic Calorimeter. *J. Chem. Eng. Data* **2005**, *50*, 270–273.

(19) Kissinger, H. E. Reaction kinetics in differential thermal analysis. *Anal. Chem.* **1957**, *29*, 1702–1706.

(20) Ozawa, T. A new method of analyzing thermogravimetic data. *Bull. Chem. Soc. Jpn.* **1965**, *38*, 1881–1886.

(21) Friedman, H. L. Kinetics of thermal degradation of char-forming plastics from thermo-gravimetry. Applications to a phenol plastic. *J. Polym. Sci.* **1963**, *6C*, 183–195.

(22) Pittayagorn, N.; Chanaiporn, D.; Banjong, B. Thermodynamic and Kinetic Properties of the Formation of $Mn_2P_2O_7$ by Thermal Decomposition of $Mn(H_2PO_2)_2{\cdot}H_2O$. *J. Chem. Eng. Data* **2009**, *54*, 871–875.

(23) Hu, R. Z. Shi, Q. Z. *Thermal analysis kinetics*; Chinese Science Press, 2001; *1st* version, pp 99−100.

(24) Banjong, B. Kinetics and Thermodynamic Properties of the Thermal Decomposition of Manganese Dihydrogenphosphate Dihydrate. *J. Chem. Eng. Data* **2008**, *53*, 1533–1538.

(25) Li, H. Q.; Shao, T. M.; Li, D. S.; Chen, D. R. Nonisothermal reaction kinetics of diasporic bauxite. *Thermochim. Acta* **2005**, *427*, 9–12.

(26) Wang, S. X.; Zhao, Z.; Tan, Z. C.; Li, Y. S.; Tong, B.; Shi, Q.; Li, Y. Thermal stability and kinetics of thermal decomposition for protinonamide. *Acta Phys. Chim. Sin.* **2007**, *23*, 1459–1462.

(27) Zhang, J. Q.; Gao, H. X.; Su, L. H.; Hu, R. Z.; Zhao, F. Q.; Wang, B. Z. Non-isothermal thermal decomposition reaction kinetics of 2-nitroimino-5-nitro-hexahydro-1,3,5-triazine (NNHT). *J. Hazard. Mater.* **2009**, in press.

(28) Montserrat, S.; malek, J.; Colomer, P. Thermal degradation kinetics of epoxy-anhydride resins: I. Influence of a silica filler. *Thermochim. Acta* **1998**, *313*, 83–95.


Received for review March 20, 2009. Accepted June 30, 2009. This work was financially supported by the Talented Personnel Funds for Scientific Research of Dalian University of Technology, China, under the grant No. 893110.

JE900285W